Available at www.sciencedirect.com

ScienceDirect

journal homepage: www.elsevier.com/locate/he

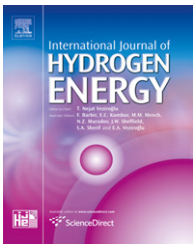

Hydrogen-induced transformation superplasticity in zirconium

Eunji Hong [a], *David C. Dunand* [b], *Heeman Choe* [a,*]

[a] *School of Advanced Materials Engineering, Kookmin University, Jeongneung-dong, Songbuk-ku, Seoul 136-702, South Korea*
[b] *Department of Materials Science and Engineering, Northwestern University, Evanston IL 60208, USA*

ARTICLE INFO

Article history:
Received 8 February 2010
Received in revised form
17 March 2010
Accepted 18 March 2010
Available online 21 April 2010

Keywords:
Hydrogen
Zirconium
Superplastic deformation
Hydride
Mechanical properties

ABSTRACT

Commercially-pure zirconium is alloyed and dealloyed repeatedly with hydrogen at 810 °C, thereby cyclically triggering phase transformations between hydrogen-free α-Zr and hydrogen-alloyed β-Zr. Under an externally applied tensile stress, the internal mismatch stresses produced by the α-β transformations are biased, resulting in the accumulation of strain increments after each chemical cycle in the direction of the applied stress. Two key parameters, i.e., half-cycle time and applied stress, are examined to determine their effects on the strain increments. A tensile strain of 133% is achieved without fracture after multiple chemical cycles, demonstrating for the first time transformation superplasticity in zirconium induced by isothermal hydrogen cycling.

1. Introduction

The interaction of metals with hydrogen is of interest for two main reasons: to develop solid hydrogen storage systems [1–5], and to allay concerns regarding the degradation of the mechanical properties in hydrogen-containing alloys for structural applications, which is known as hydrogen embrittlement [6–9]. In particular, zirconium and its alloys have been examined by various researchers as hydrogen carriers [1,2,10] and for structural metallic systems with concerns in the deterioration of the mechanical properties [6–8,11,12]. The latter is particularly well studied, as zirconium alloys are used in nuclear reactors, owing to their low neutron absorption, good corrosion resistance, and good mechanical properties [6,12]. For example, Zircaloy-4 (Zr-1.5Sn-0.2Fe-0.1Cr) is used widely as cladding for uranium fuel to protect against deterioration from the flowing coolant [6,13–15]. However, as a result of its interaction with coolant water, zircaloy is subject to hydrogen uptake during operation. This is undesirable, since the high diffusivity of hydrogen and the formation of zirconium hydride phases in the alloy lead to the deterioration of their mechanical properties. Also at lower levels of hydrogen, before hydride formation, zirconium and its alloys undergo a phase transformation from α-Zr to β-Zr. Rapid deformation can occur when an external stress is applied during a phase transformation and this transformation mismatch plasticity (TMP) may be of concern during reactor operation.

On the other hand, TMP can be harnessed to achieve very large deformation at low stresses when numerous phase transformations are triggered by cyclically charging and discharging the material with hydrogen at elevated temperatures. Transformation mismatch plasticity (TMP) and the closely related internal-stress plasticity (ISP) are used to

* *Corresponding author*. Tel.: +82 2 910 4417; fax: +82 2 910 4320.
E-mail address: heeman@kookmin.ac.kr (H. Choe).
0360-3199/$ – see front matter © 2010 Professor T. Nejat Veziroglu. Published by Elsevier Ltd. All rights reserved.
doi:10.1016/j.ijhydene.2010.03.088

increase the deformation rate of various metals, alloys, and ceramics undergoing deformation by creep or low-temperature plasticity, as reviewed in Ref. [16]. When mismatch stresses or strain are produced during the phase transformation between two coexisting allotropic phases with different densities, they can be biased in the direction of the external stress, resulting in a strain increment in the same direction as the biasing stress, with a magnitude proportional to the biasing stress [17–19]. If the internal mismatch is regenerated constantly during cyclical phase transformation, the average strain rate is proportional to the applied stress: the average strain rate sensitivity is then unity, corresponding to Newtonian flow and exceptional flow stability [20]. This can result in tensile strain well in excess of 100%, in a phenomenon known as internal-stress superplasticity or transformation superplasticity [16].

Although cycling the temperature around a phase transformation temperature is the most common technique to produce the reproducible internal stresses needed to generate superplastic deformation (as demonstrated, e.g., in titanium [19,21–25] and zirconium alloys [26,27]), hydrogen cycling at a constant temperature can also produce transformation superplasticity in titanium [26,28–31] or internal-stress plasticity in palladium [32]. For pure α-titanium, the very high diffusivity of hydrogen allow for rapid hydrogen charging by exposure to a hydrogen-bearing atmosphere, which leads to the formation of the β-Ti phase [28,33]. The hydrogen is then rapidly discharged upon exposure to a vacuum or a hydrogen-free atmosphere, resulting in a transformation back to the α-Ti phase. Because this new method uses hydrogen to induce internal-stresses at constant temperature, it has been called "chemically induced internal-stress plasticity", as opposed to the more common thermally induced plasticity [28].

This paper demonstrates that superplastic deformation can be achieved in pure zirconium by repetitive hydrogen charging and discharging at constant temperature, similarly to temperature cycling without hydrogen [26,27]. It is thus relevant to our understanding of deformation of zirconium which can be desirable (e.g., during a forming operation) or undesirable (e.g., during unplanned hydrogen exposure). It also provides some insight in the development of solid hydrogen storage systems using zirconium hydrides as hydrogen carriers.

2. Experimental procedures

Cylindrical specimens of commercially-pure zirconium (>99.2% pure, United Titanium Inc., Ohio) were machined with a gauge length and gauge diameter of 30.0 mm and 3.0 mm, respectively. The threaded specimen heads had a length and diameter of 5 mm and 4 mm, respectively, which is only slightly larger than the gauge diameter of 3.0 mm to avoid their possible role as hydrogen sinks/sources during charge/discharge [31].

The experiments were carried out at 810 °C in a custom-built machine (Fig. 1), which can perform reversible hydrogen cycling under small tensile stresses at elevated temperatures in a gas atmosphere [26]. The entering gas, with a flow rate of 6 L/min, could be changed from high-purity

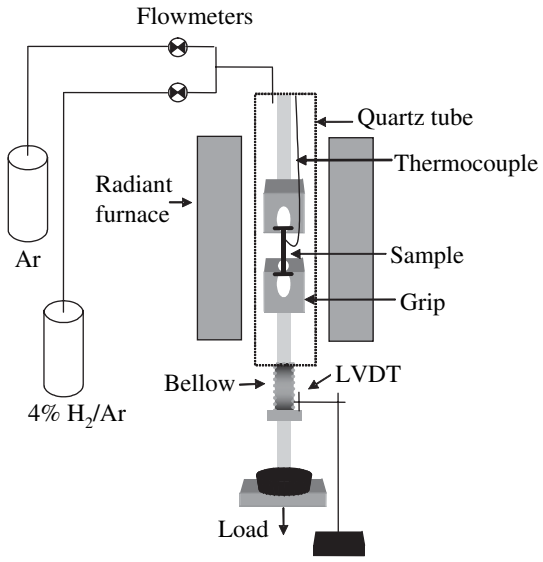

Fig. 1 – Schematic of the custom-built machine used to measure strain under cyclic hydrogen atmosphere, for a sample subjected to a constant tensile stress at elevated temperature.

99.999% Ar to a gas mixture of 4% H_2 in Ar using a premixed gas tank. The hydrogen partial pressure used for all experiments was 450 Pa, corresponding roughly to ~6 at. %, which is well past the solvus line between the α-Zr + β-Zr field and the β-Zr field based on the published Zr-H phase diagram (Fig. 2). The temperature was raised to 810 °C at the rate of 10 °C/min. and was held at that temperature for 10 min before starting each test. Prior to each measurement, the specimens were pre-exposed to the Ar atmosphere for 10 min. For every experiment, 5–7 consecutive chemical cycles were performed and the average specimen length changes were calculated without the first cycle as the dynamic equilibrium state is normally reached after the first or second cycle [2,31]. Caution was exercised to minimize zirconium oxidation on the hydrogen charging/discharging experiments. A new sample was used in each experiment whenever there appeared to be

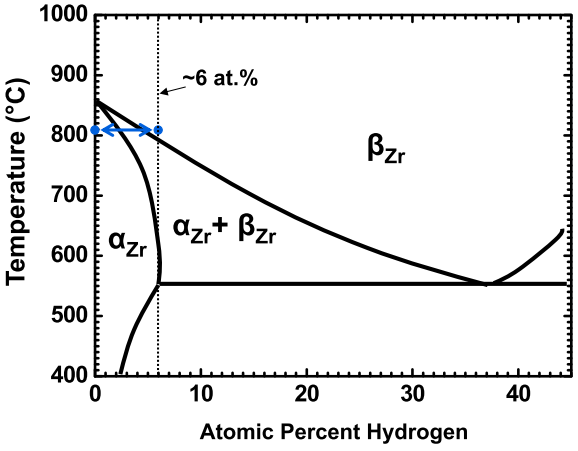

Fig. 2 – Zirconium-hydrogen phase diagram [34] showing the chemical cycling used in this study to induce transformation mismatch plasticity at 810 °C.

degradation in the hydrogen absorbing capacity, which generally did not occur before ~15 h of high-temperature exposure. The changes in gauge length were measured using an external linear voltage-displacement transducer (LVDT) at the cold end of the load train. More experimental details can be found elsewhere [28].

3. Results and discussion

Fig. 3 shows a typical strain history during hydrogen charging/discharging cycling with a half cycle time of 10 min and a stress of 3.1 MPa. The cyclic oscillations in the curve corresponded to a combination of strain increment and decrement processes during hydrogen charging/discharging, due to reversible lattice swelling from hydrogen dissolution, high-temperature creep deformation, and zirconium phase transformation [28,31]. A plastic strain increment of 2.5 pct was obtained for each cycle, corresponding to an average strain rate of 2.1×10^{-5}/s for the cycle frequency of 3.0/h.

The magnitude of volume mismatch which can be obtained by lattice swelling is much greater than that from the phase transformation mismatch. For example, the magnitude of the swelling volume mismatch in pure Ti, which is attributed mainly to deformation in the weaker β phase, was approximately four times higher than that of the transformation volume mismatch at 860 °C [28,29,35]. From the phase diagram in Fig. 2, the estimated hydrogen composition that is sufficient to minimize lattice swelling mismatch, but can still allow complete TMP to occur, is ~6 at %. The literature data indicates that the corresponding equilibrium partial pressure of hydrogen can range from ~47 to 695 Pa with an average value of ~404 Pa, according to Sieverts' law [14]:

$$P_{H_2} = \left(\frac{C_{eq}}{K_H}\right)^2 \quad (1)$$

where P_{H_2} is the hydrogen partial pressure, C_{eq} is the equilibrium amount of absorbed hydrogen, K_H is the Sieverts constant, and T is the absolute temperature. Fig. 4 shows the stress dependence of the average strain increment accumulated for hydrogen chemical charging/discharging with a hydrogen partial pressure, frequency, and half cycle time of ~450 Pa, 3 h^{-1}, and 10 min, respectively. The partial pressure of ~450 Pa was assumed to be sufficient or near sufficient for α- to β-phase transformation with insignificant swelling effect, if any. The strain increment per cycle shows linear behavior with a slope of ~14 GPa^{-1} at lower stresses up to ~2.6 MPa, beyond which a rapid, non-linear increase in strain increment occurs, as reported in other studies [28,31]. The linear region can be extrapolated to a strain of −1.4% for zero stress. This chemical ratcheting strain is of the same sign, but higher by an order of magnitude than that measured during ratcheting of titanium [29]. Direct comparison is difficult, as these experiments were carried out at 860 °C on specimens with shorter aspect ratios. Also plotted in Fig. 4 is the creep strain accumulated for β-Zr at 810 °C for 20 min (the time for a complete H-charging/discharging cycle) estimated roughly using the creep parameters of β-Zr reported in Ref. [36]. These strains are insignificant as compared to the TMP strains for the stress range studied here. Also compared is the creep data of β-Zr 705 alloy at 900 °C, a much higher temperature than the current testing temperature, still showing smaller strains accumulated at higher stress levels [27].

Finally, reproduced in Fig. 4 are the strain increments for thermal cycling between 810 and 940 °C as measured experimentally for Zr at a frequency of 30 h^{-1} [26], an order of magnitude higher than the one used for chemical cycling in the present experiments. Although the TMP strains are generally larger for chemical cycling than for thermal cycling

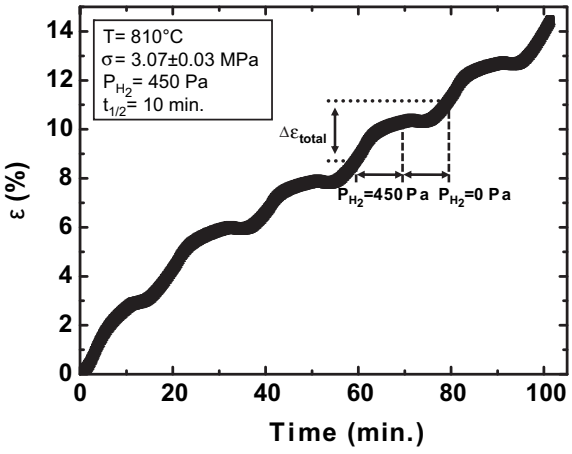

Fig. 3 – Strain history of Zr during five consecutive hydrogen charging/discharging cycles ($P_{H_2} = 0 \leftrightarrow 450$ Pa) at 810 °C and for an applied stress of 3.1 MPa, with 10 min half cycles. The hydrogen charging and discharging segments are shown specifically for the 4th cycle.

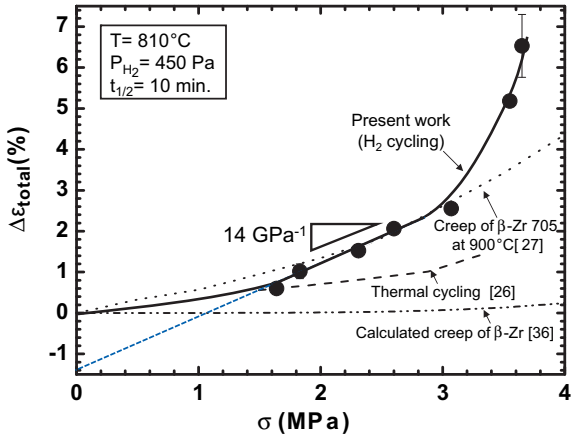

Fig. 4 – Average strain increment accumulated in Zr for hydrogen charging/discharging cycles ($P_{H_2} = 0 \leftrightarrow 450$ Pa) with 10 min half cycle time as a function of applied stress at 810 °C (error bars are one standard deviation and smaller than symbols, except for highest stress). Also shown for comparison are data for thermal cycling (T = 810–940 °C, 1 min half cycle time) for pure Zr [26], the creep strain increment calculated using the creep parameters of β-Zr at 810 °C [36], as well as the creep strain increment calculated from the creep data of β-Zr 705 alloy measured at 900 °C [27].

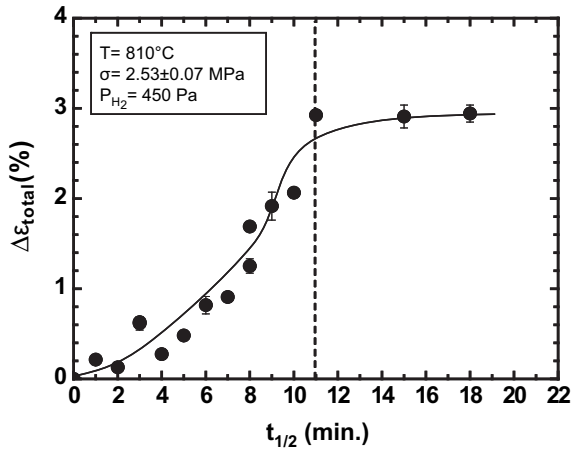

Fig. 5 – Strain increment per charging/discharging cycle (P_{H_2} = 0 ↔ 450 Pa) as a function of the half cycle period, for Zr at 810 °C and 2.5 MPa.

at a given stress, because of the additional swelling effect [23,28], it is difficult to compare these two types of TMP strains directly for the following reasons. First, the transformation temperature between the α- and β-phases is 53 °C lower for chemical cycling than for thermal cycling (810 vs. 863 °C), so that the weaker phase accommodating mismatch during the phase transformation (β-Zr) deforms more slowly in the former case, thus decreasing the strain increment [37]. Second, the half cycle time used for thermal cycling is only 1 min, which is an order of magnitude lower than that for chemical cycling, so that internal mismatch stresses are higher, and internal strains decay less fully during the phase transformation. Third, hydrogen-induced TMP depends on the complex motion of the α/β phase boundary, causing highly inhomogeneous stresses localized in regions near the transformation front [38]. This is in contrast to temperature-induced TMP, for which transformation occurs by nucleation and growth of numerous β grains homogenously distributed within the volume of the sample.

Fig. 5 reports the results of a series of experiments where the half cycle time $t_{1/2}$ was varied from 1 to 18 min while keeping the other variables constant (σ = 2.53 MPa, P_{H_2} = 450 Pa, T = 810 °C). The strain increment increases almost linearly up to $t_{1/2} \sim 11$ min, after which it is near constant. It thus appears that the minimum half-cycle time required for complete transformation in the present samples through the charging and discharging of hydrogen is ~11 min, which is in contrast to the half-cycle time of 5 min reported for the complete transformation of commercially-pure Ti with the same sample dimensions at a lower pressure P_{H_2} = 200 Pa and higher temperature T = 860 °C [31]. After a complete transformation is obtained at the half-cycle time of ~11 min, the sample experiences an insignificant amount of excess creep deformation, which is characterized by the plateau in Fig. 5. The half cycle time for complete transformation without swelling can also be estimated analytically as [38]:

$$t^*_{1/2} \approx \frac{Ta^2}{D_\alpha} \tag{2}$$

where T is the dimensionless time, D_α is the diffusion coefficient, and a is the radius of a sample. The dimensionless critical transformation time, T, was calculated to range from 0.23 to 2 (Eq. (3)), according to the range in C_S^β (~4.2–~5.7 at.%) obtained from several different Zr-H phase diagrams [34,39,40] based on [38]:

$$T \approx T_C^\alpha \approx X \cdot \left(1 - C_S^\alpha\right) \cdot \left(\frac{1 - C_S^\beta}{C_S^\beta}\right)^{-C_S^{\alpha Y}} \cdot \Phi^{\left(1-C_S^\alpha\right)^Z} \tag{3}$$

where T_C^α is the critical transformation time for phase α, C_S^p is concentration at the moving phase boundary in phase P, Φ is ratio of diffusivities, and X, Y, and Z are geometry constants. Taking the values for the radius of a specimen, a = 1.5 mm and $D_\alpha = 4.2 \times 10^{-5}$ cm^2/s (calculated as $D_0 \exp(-Q/RT)$ with $D_0 = 2.9 \times 10^{-3}$ cm^2/s and $Q = -38.1 \pm 1.4$ kJ/mol [41]), $t_{1/2}{}^*$ also varied from ~2 to 18 min, which is roughly consistent with the experimental value of ~11 min from Fig. 5. The linear behavior of a strain increment below $t_{1/2}{}^* \sim 11$ min is expected, as the transformation is partially complete in that region. The near zero slope for $t_{1/2} > \sim 11$ min further confirms that swelling effects are minimal after a full transformation is achieved at 450 Pa H_2.

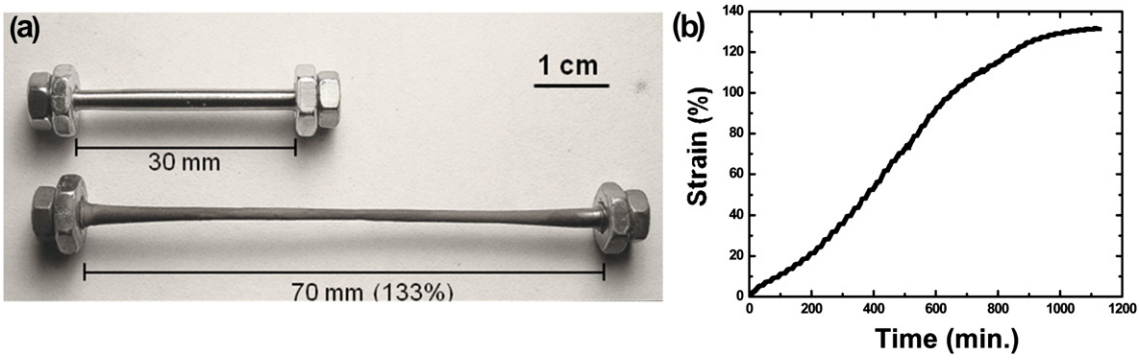

Fig. 6 – (a) Photograph of an undeformed Zr sample and a sample deformed to an engineering strain of e = 133% after 47 hydrogen cycles (P_{H_2} = 0 ↔ 450 Pa) at 810 °C. The stress was held at a constant 2.4 ± 0.06 MPa value during the entire test. Two steel nuts were screwed at each sample head to provide a grip for the load train. (b) The corresponding strain history of Zr during the superplasticity test.

Based on the parametric studies shown in Figs. 4 and 5, the following parameters were selected to demonstrate the superplastic behavior (defined here as a tensile strain in excess of 100%): 12 min half-cycle time and a stress of 2.4 ± 0.06 MPa (maintained constant by periodically reducing the force on the sample because of its decreasing cross-section, calculated by volume conservation). After 47 complete cycles, a pure zirconium sample achieved an engineering strain of $e = 133\%$ without significant necking or fracture, as shown in Fig. 6(a). The average strain per cycle was 1.9%, which is lower than the value of 2.7% expected from the result in Fig. 5. This is due to the lower strain increments accumulated at the end of the test, as shown in Fig. 6(b). On the contrary, the average stain per cycle up to 900 min was 2.6%, similar to that of the value estimated from the result in Fig. 5. The total strain increases approximately linearly up to 900 min, after which it gradually tapers off as the number of cycles increases, as shown in Fig. 6(b). This leveling of the strain in the final part of the strain history curve in Fig. 6(b) can be attributed to the incomplete H-charging/discharging caused by the formation of oxide on the specimen surface [15], as indicated by the darker color of the tested specimen compared to the untested one (Fig. 6(a)). On the other hand, in Zr-based compounds used for hydrogen storage, such as ZrNi, the hydrogen absorbing capacity is degraded after multiple hydriding/dehydriding cycles, due to the phase decomposition and microstructural changes [2].

4. Conclusions

The formation of hydrides in zirconium alloys can be of interest for various reasons, from storing hydrogen to degrading zirconium mechanical properties. Here, we studied the effect of hydrogen alloying/dealloying – a necessary step to form hydrides in zirconium – upon pure zirconium subjected to a tensile stress at 810 °C. We examined the case where ~6 at % H is added to Zr (P_{H_2} = ~450 Pa), which is assumed to be sufficient or near sufficient to trigger the α–β transformation with minimal hydrogen-induced swelling of β-Zr, thus focusing on the effect of volume mismatch during the phase transformation under stress. The strain increment after a hydrogen cycle increased linearly with applied stress (at low stresses of 1–3 MPa), indicative of transformation mismatch plasticity. Additionally, the strain increment increased near linearly with the cycling period, as expected for a diffusion-controlled process. Transformation superplasticity was demonstrated in a sample which accumulated a total engineering strain of 133% without fracture after 47 chemical cycles under a stress of 2.4 MPa.

Acknowledgments

This work was carried out under the Nuclear R&D Program supported by Ministry of Knowledge Economy, Republic of Korea. HC also acknowledges support from the Priority Research Centers Program through the National Research Foundation of Korea (NRF) funded by the Ministry of Education, Science and Technology (2009-0093814).

REFERENCES

[1] Zidan RA, Takara S, Hee AG, Jensen CM. Hydrogen cycling behavior of zirconium and titanium-zirconium-doped sodium aluminum hydride. J Alloys Compd 1999;285:119–22.
[2] Simonović BR, Mentus S, Dimitrijević R, Šušić MV. Multiple hydriding/dehydriding of $Zr_{1.02}Ni_{0.98}$ alloy. Int J Hydrogen Energy 1999;24:449–54.
[3] Jalowiecki-Duhamel L, Carpentier J, Ponchel A. Catalytic hydrogen storage in cerium nickel and zirconium (or aluminium) mixed oxides. Int J Hydrogen Energy 2007;32:2439–44.
[4] Takasaki A, Kelton KF. Hydrogen storage in Ti-based quasicrystal powders produced by mechanical alloying. Int J Hydrogen Energy 2006;31:183–90.
[5] Sakintuna B, Lamari-Darkrim F, Hirscher M. Metal hydride materials for solid hydrogen storage: a review. Int J Hydrogen Energy 2007;32:1121–40.
[6] Kim JH, Lee MH, Choi BK, Jeong YH. Effect of the hydrogen contents on the circumferential mechanical properties of zirconium alloy claddings. J Alloys Compd 2007;431:155–61.
[7] Khatamian D, Ling VC. Hydrogen solubility limits in α- and β-zirconium. J Alloys Compd 1997;253–254:162–6.
[8] Ivanova SV. Effect of hydrogen on serviceability of zirconium items in VVER and RBMK-type reactors fuel assemblies. Int J Hydrogen Energy 2002;27:819–24.
[9] Michler T, Naumann J. Hydrogen embrittlement of Cr-Mn-N-austenitic stainless steels. Int J Hydrogen Energy 2010;35:1485–92.
[10] Bouhadda Y, Radehi A, Boudouma Y, Fenineche N, Drabila S, Meradji H. Hydrogen solid storage: first-principles study of $ZrNiH_3$. Int J Hydrogen Energy 2009;34:4997–5002.
[11] Ivanona SV. Hydrogen effected defects evolution in zirconium items of light-water reactors. Int J Hydrogen Energy 2006;31:295–300.
[12] Ivanova SV. Effect of hydrogen on serviceability of zirconium items in VVER and RBMK-type reactors fuel assemblies. Int J Hydrogen Energy 2002;27:819–24.
[13] Yamanaka S, Setoyama D, Muta H, Uno M, Kuroda M, Takeda K, et al. Characteristics of zirconium hydrogen solid solution. J Alloys Compd 2004;372:129–35.
[14] Yamanaka S, Higuchi K, Miyake M. Hydrogen solubility in zirconium alloys. J Alloys Compd 1995;231:503–7.
[15] Elmoselhi MB. Hydrogen uptake by oxidized zirconium alloys. J Alloys Compd 1995;231:716–21.
[16] Nieh TG, Wadsworth J, Sherby OD. Superplasticity in metals and ceramics. Cambridge, UK: Cambridge University Press; 1997.
[17] Greenwood GW, Johnson RH. The deformation of metals under small stresses during phase transformation. Proc Roy Soc Lond A 1965;283:403–22.
[18] Schuh C, Dunand DC. Contributions to transformation superplasticity of titanium from rigid particles and pressurized pores. Scripta Mater 1999;40:1305–12.
[19] Dunand DC, Bedell CM. Transformation-mismatch superplasticity in reinforced and unreinforced titanium. Acta Mater 1996;44:1063–76.
[20] Schuh C, Dunand DC. Non-isothermal transformation-mismatch plasticity: modeling and experiments on Ti-6Al-4V. Acta Mater 2001;49:199–210.
[21] Schuh C, Dunand DC. Tensile fracture during transformation superplasticity of Ti-6Al-4V. J Mater Res 2001;16:865–75.
[22] Dunand DC, Myojin S. Biaxial deformation of Ti-6Al-4V and Ti-6Al-4V/TiC composites by transformation-mismatch superplasticity. Mater Sci Eng A 1997;230:25–32.

[23] Murray NGD, Schuh C, Dunand DC. Solid-state foaming of titanium by hydrogen-induced internal-stress plasticity. Scripta Mater 2003;49:879–83.
[24] Frary M, Schuh C, Dunand DC. Kinetics of biaxial dome formation by transformation superplasticity of titanium alloys and composites. Metall Mater Trans A 2002;33: 1669–80.
[25] Schuh C, Noel PA, Dunand DC. Enhanced densification of metal powders by transformation-mismatch plasticity. Acta Mater 2000;48:1639–53.
[26] Zwigl P, Dunand DC. Transformation superplasticity of zirconium. Metall Mater Trans A 1998;29:2571–82.
[27] Gonzalez HJ, Dunand DC. Transformation superplasticity in zircadyne 705. J Mater Eng Perform 2004;13:665–9.
[28] Zwigl P, Dunand DC. Internal stress plasticity in titanium by cyclic alloying/dealloying with hydrogen. J Mater Proc Tech 2001;117:409–17.
[29] Frary M, Schuh C, Dunand DC. Strain ratcheting of titanium upon reversible alloying with hydrogen. Phil Mag A 2001;81: 197–212.
[30] Dunand DC, Zwigl P. Hydrogen-induced internal stress plasticity in Titanium. Metall Mater Trans A 2001;32: 841–7.
[31] Choe H, Schuh C, Dunand DC. Superplastic deformation induced by cyclic hydrogen charging. J Appl Phys 2008;103. 103518(1–9).
[32] Beeri O, Dunand DC. Transformation mismatch plasticity in Pd induced by cyclic hydrogen charging. Mater Sci Eng A 2009;523:178–83.
[33] Zhang X, Zhao Y, Zeng W. Effect of hydrogen on the superplasticity of Ti600 alloy. Int J Hydrogen Energy 2010;35: 4354–60.
[34] Zuzek E, Abriata JP, San-Martin A, Manchester FD. The H-Zr (Hydrogen-Zirconium) system. Bull Alloy Phase Diagrams 1990;11:385–95.
[35] McCoy HE. Trans ASM 2001;57:743–6.
[36] Sargent PM, Ashby MR. Deformation maps for titanium and zirconium. Scr Metall 1982;16:1415–22.
[37] Schuh C, Dunand DC. Transformation superplasticity of super α_2 titanium aluminide. Acta Mater 1998;46:5663–75.
[38] Schuh C. Modeling gas diffusion into metals with a moving-boundary phase transformation. Metall Mater Trans A 2000; 31. 2411–21.
[39] Dupin N, Ansara I, Servant C, Toffolon C, Lemaignan C, Brachet JC. A thermodynamic database for zirconium alloys. J Nucl Mater 1999;275:287–95.
[40] Setoyama D, Yamanaka S. Phase diagram of Zr-O-H ternary system. J Alloys Compd 2003;370:144–8.
[41] Shmakov AA, Singh RN. Some peculiarities of hydrogen behavior and delayed hydride cracking in zirconium based reactor alloys. In: Invited talk at SAM-CONAMET 2009;19 Buenos Aires. Argentina.